Springer

KSME

Journal of Mechanical Science and Technology 30 (4) (2016) 1773~1779
www.springerlink.com/content/1738-494x(Print)/1976-3824(Online)
DOI 10.1007/s12206-016-0333-0

Welding residual stress analysis of 347H austenitic stainless steel boiler tubes using experimental and numerical approaches †

Wanjae Kim*, Kwang Soo Kim, Hansang Lee and Keunbong Yoo

KEPRI, Munjiro 105, Yusunggu, Daejeon, Korea

(Manuscript Received June 3, 2015; Revised September 22, 2015; Accepted November 30, 2015)

Abstract

A three-dimensional finite element model that can simulate multiple start/stop welding process of 347H austenitic stainless steel boiler tubes was developed to estimate welding residual stress distributions. Two-dimensional axisymmetric finite element model and three-dimensional finite element model that exhibit half symmetry along circumferential direction are also employed for verification purposes. Sequentially coupled thermo-mechanical finite element analyses were carried out using three different models to obtain and compare temperature fields and resulting residual stress fields. In addition, node-based temperature heat input method and element-based body flux heat input method were applied to three-dimensional half symmetry model to review the adequacy of heat input model that can best estimate welding residual stress distribution in the tubes. Finally, welding residual stresses obtained using different models were compared with measured data, and it was observed that results using three-dimensional finite element model that can take into account welding start/stop effects are in good agreement with those of measured data obtained by the X-ray diffraction (XRD) method.

Keywords: Welding residual stress; 347H; Boiler tubes; X-ray diffraction; Finite element method

1. Introduction

347H austenitic stainless steel has been widely used in the power generation industry because of its superior creep properties [1]. Several cases of 347H boiler tube failure in welded region have been reported and failure cases seem to be an increasing trend. Elevated steam temperature is the main cause of the failure. However, temperature increase is unavoidable because it is directly connected to plant power output increase. Preventive measures as Post-weld heat treatment (PWHT) are applied to mitigate observed damage phenomenon. Design of PWHT often encompasses a wide range of complicated processes, including selection of heating method, range, holding time and temperature and so on. Evaluation of welding residual stresses plays an important role in PWHT planning for detailed heat treatment design process can be referenced to present residual stress profile.

Numerical welding simulations have become widely adopted in predicting weld induced deformation and residual stresses. As computing power develops exponentially, numerical approaches have proved to be a very powerful tool to predict weld-induced material behavior. However, numerical welding simulation demands rather expensive computational cost, in other words, simulation requires large storage space and computing time, and solving large-scale three-dimensional welding simulations which, in particular, have multiple welding passes still remains as a challenge. Therefore, recent studies mainly focus on reducing computing cost while maintaining accuracy to acceptable levels [2, 3]. Jie Xu et al. [4] employed three-dimensional and axisymmetric finite element models to estimate welding residual stresses in pipes. This work highlights discrepancies that can be observed when simplified models are used. Barsoum et al. [5] proposed simplified two-dimensional models and compared CPU times with those spent by three-dimensional models. This work summarizes how a well defined two-dimensional model can save computation cost under such condition that 3D effects can be neglected. Vakili-Tahami et al. [6] adopted a double ellipsoidal heat source model to obtain temperature field and stress field using two- and three-dimensional finite element models. This work concludes that two-dimensional models can only be used to predict temperature distribution. Long Tan et al. [7] investigated pass lumping effects using a two-dimensional axisymmetric model and suggested that well defined lumped pass model can reduce computation cost without sacrificing accuracy too much.

Some other works investigated three-dimensional effects caused mainly by weld torch start/stop between welding passes. Dong et al. [8] emphasized discrepancies in residual

*Corresponding author. Tel.: +82 42 865 5623, Fax.: +82 42 865 5639
E-mail address: wj.kim@kepco.co.kr
† Recommended by Associate Editor Beomkeun Kim

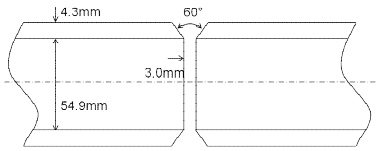

Fig. 1. Dimensions of weld tube.

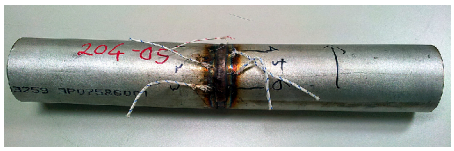

Fig. 2. Girth-welded SUS347H mock-up.

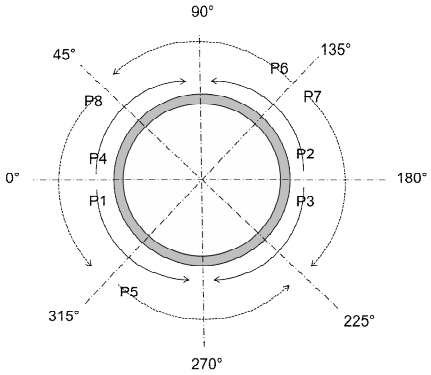

Fig. 3. Welding sequence and start/stop position.

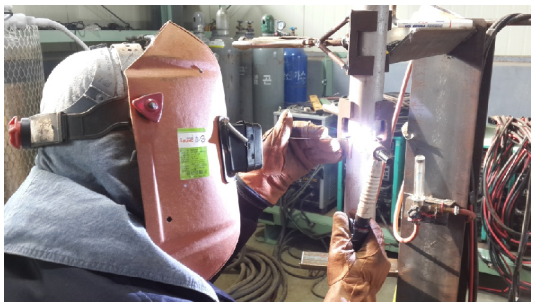

Fig. 4. Test rig setup and mock-up welding.

stress distributions observed in two weld regions, one in steady range and the other is near the weld start/stop region.

In this work, a finite element model was developed to predict welding residual stresses in an SUS347H two-pass girth welded boiler tube that has total eight start/stop regions. In addition, a two-dimensional axisymmetric model and three-dimensional model that has half symmetry along circumferential direction are employed to emphasize the importance of considering three-dimensional effects in welding residual stress evaluation. Node-based temperature heat input method and element-based body flux heat input method are adopted to review the adequacy of heat input model that can best estimate welding residual stress distribution in the tubes. Welding residual stresses obtained using different models are then compared with those by X-ray diffraction (XRD) method and then

Table 1. Welding parameters.

Layer	Type	Current [A]	Voltage [V]	Speed [mm/s]
1st layer	GTAW	90	12	0.67
2nd layer	GTAW	100	14	0.89

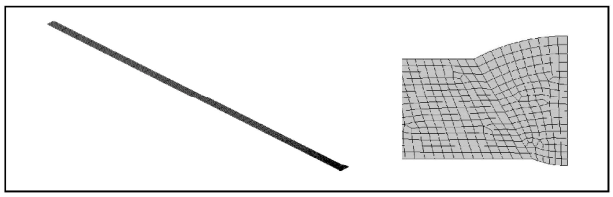

(a) Model a. Two-dimensional axi-symmetric model

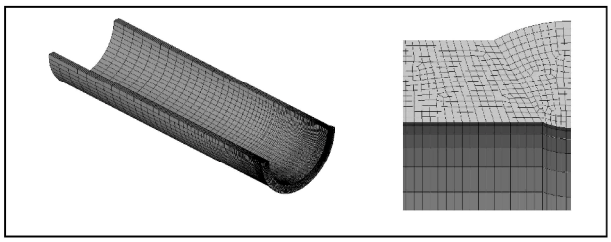

(b) Model b. Three-dimensional half model

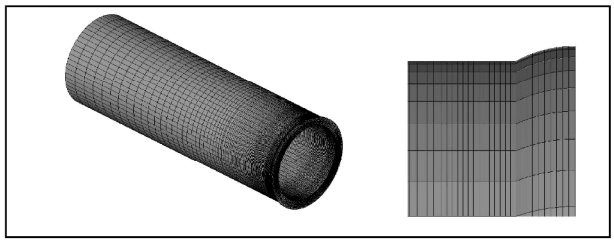

(c) Model c. Three-dimensional full model

Fig. 5. Finite element models for welding simulation.

results are validated.

2. Description on SUS347H mock-up

A mock-up was manufactured to measure temperature histories and residual stresses. Dimensions and groove shape are shown in Fig. 1. Length of the mock-up is 390 mm. Welding sequence is depicted in Fig. 3. P1 to P8 represent weld passes and the mock-up was manufactured by these eight weld passes. First four passes form the first layer of the mock-up and the other passes form the second layer. Gas tungsten arc welding (GTAW) was used in the experiment and the filler metal was the same as parent material, 347H. Welding parameters are shown in Table 1. Two weld layers are formed using the same welding method, GTAW. For the first layer, welding current, voltage and speed are 90 A, 12 V and 0.67 mm/s, respectively, and for the second layer, welding current, voltage and speed are 100 A, 14 V and 0.89 mm/s. Fig. 4 shows a test rig used to manufacture the mock-up. Tube was held in vertical position during welding and fixed at upper end section. After welding,

Table 2. Finite element model data.

FE model	# of Node	# of Element	Thermal	Mechanical
2D axisymm.	1129	1018	DCAX4	CAX4
3D half	34999	30540	DC3D8	C3D8
3D full	67740	61080	DC3D8	C3D8

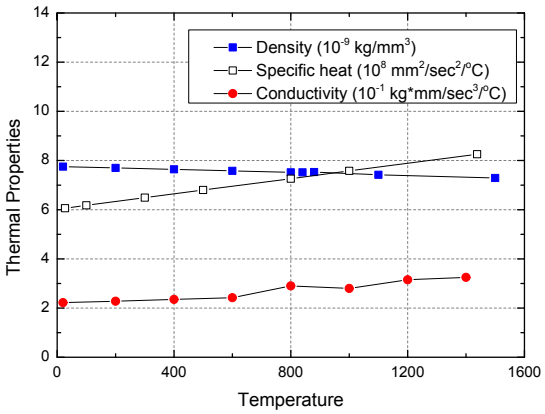

Fig. 6. Temperature-dependent thermal properties of SUS347H.

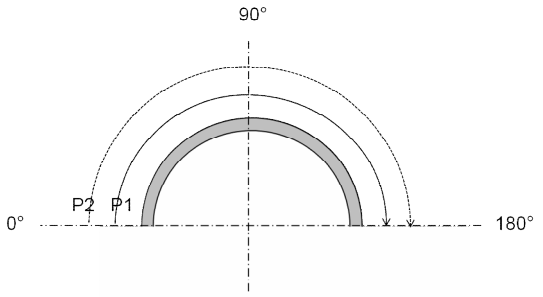

Fig. 7. Welding sequence and start/stop position for model b.

residual stresses were measured using XRD method. Detailed measurement locations are shown in the following section.

3. Finite element model

Three finite element models were developed: 1) Two-dimensional axi-symmetric model, 2) three-dimensional model that exhibits half symmetry along circumferential direction and 3) three-dimensional model that can simulate eight weld passes. The third one is considered to be the most realistic. Axial symmetry was assumed for all models since shape, load and constraints can be considered symmetric on axial plane halfway from each end.

Fig. 5 shows finite element models used for welding simulation. All models have the same dimensions and groove shape as Fig. 1. Two-dimensional axisymmetric model (Referred to as model a) has the same cross sectional mesh density as other two three-dimensional models. Model a has 1129 nodes and 1018 elements. For thermal analysis, DCAX4 element provided by commercial CAE software Abaqus was used. DCAX4 is diffusive heat transfer element which has

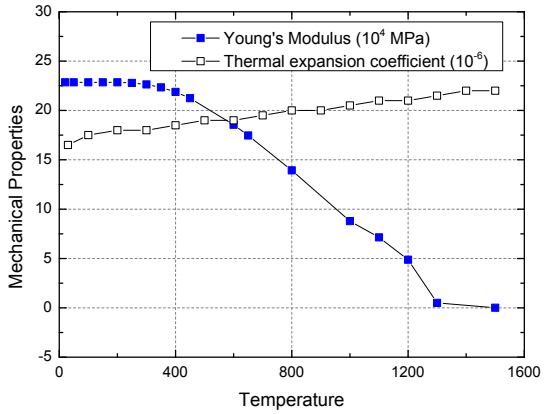

Fig. 8. Temperature-dependent mechanical properties of SUS347H.

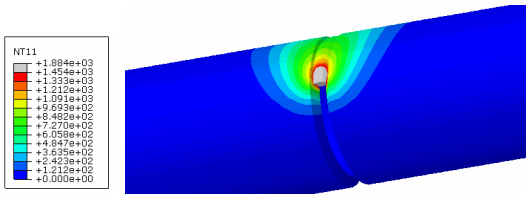

Fig. 9. Temperature distribution obtained at the end of the first weld pass in model c.

temperature degree of freedom and is able to describe axi-symmetric behavior of materials. For mechanical analysis, CAX4 element is adopted which has translational degrees of freedom in axial and radial directions. Three-dimensional half model (Referred to as model b) exhibits both axial and circumferential symmetry; therefore, it is actually a quarter of the real model used for experiment and a half of three-dimensional full model (Referred to as model c). Model b has 34999 nodes and 30540 elements. Linear brick elements, C3D8, are used both for thermal and mechanical analyses. Model c has approximately twice as many nodes and elements as model b. Number of elements in circumferential direction is 60 for model c and 30 for model b. Since all three models have the same cross sectional mesh density and for three-dimensional models, same circumferential mesh density, problems arise from using different mesh densities can be minimized. Representative finite element model data are summarized in Table 2.

4. Numerical welding residual stress calculation

To obtain temperature and stress distributions, sequentially coupled thermo-mechanical finite element analyses are carried out using models a, b and c. In contrast with coupled thermo-mechanical analysis, temperature field and stress field are calculated in a successive manner in a sequentially coupled analysis. This procedure is based on sound theoretical understanding that the amount of heat generated by plastic dissipation is negligible compared to the heat generated by weld torch.

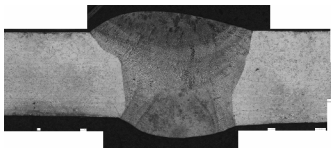

(a) Fusion zone in weld mock-up

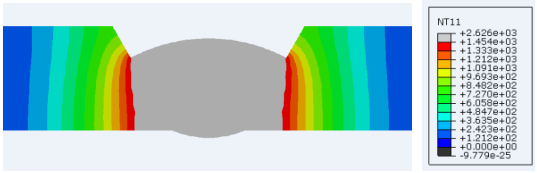

(b) Fusion zone in model a

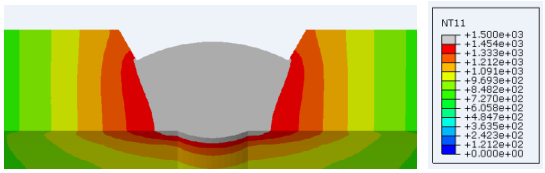

(c) Fusion zone in model b (temperature heat input)

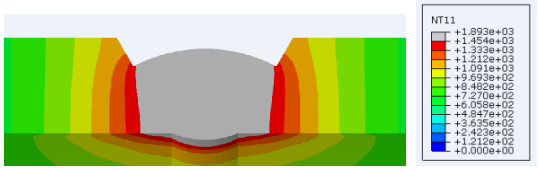

(d) Fusion zone in model b (body flux heat input)

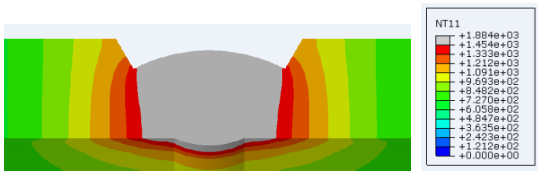

(e) Fusion zone in model c

Fig. 10. Fusion zones in various models.

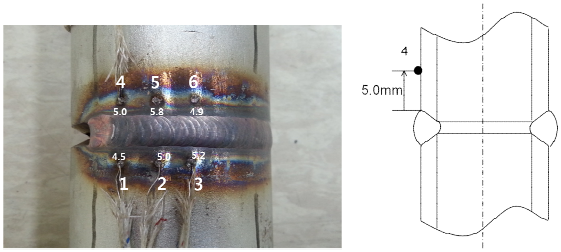

Fig. 11. Temperature measurement locations.

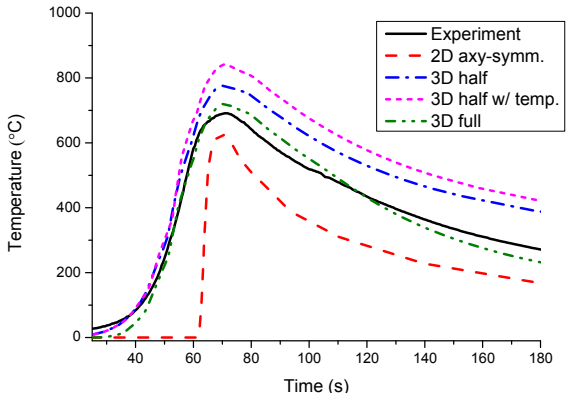

Fig. 12. Experimental and numerical temperature histories at location 4.

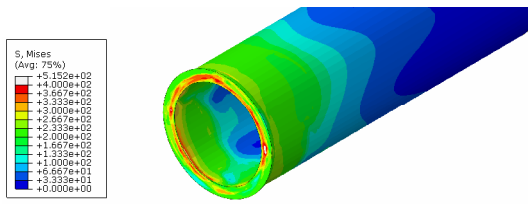

Fig. 13. Von Mises stress distribution in model c after cooling.

4.1 Thermal analysis

In the thermal analysis, model change option is adopted which can add or remove sets of elements. During the analysis, blocks of elements are sequentially added to simulate torch movement and then heated to heat input from the torch. The distributed heat flux is given by

$$q = \frac{\eta VI}{Av\Delta t} \tag{1}$$

where η is the arc efficiency, V is the voltage, I is the current, A is the cross sectional area, v is the welding speed and Δt is the heating time. Assumed welding parameters are listed in Table 1 and arc efficiency is set to be 0.67 [9]. For the present analysis, natural convection is assumed with heat convection coefficient of 20 W/m^2°C and ambient temperature is assumed to be 0°C according to recorded temperature during experiment. Temperature-dependent thermal properties used for the simulation are shown in Fig. 6. Welding sequence for model c is same as Fig. 3 and welding sequence for model b is shown in Fig. 7. 1000s is given for inter-pass cooling and 3000s is given for final cooling after torch leaves tube.

4.2 Mechanical analysis

In the mechanical analysis, the same finite element mesh is employed as used in the thermal analysis. Temperature histories computed in the previous analysis are used as input. Total strain at a point is calculated by summing up material elastic strain, plastic strain, thermal strain and strain induced by phase transformation. Since SUS347H has no metallurgical phase transformation, the last strain term can be neglected in the present work. Temperature-dependent mechanical properties employed in the simulation are shown in Fig. 8. According to the test rig setup shown in Fig. 4, clamping conditions are employed only to prevent rigid body motion.

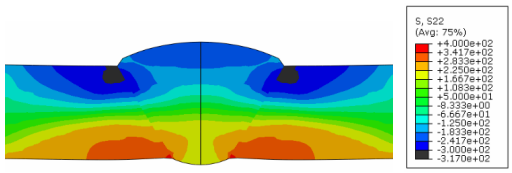

(a) Axial stress distribution in model a

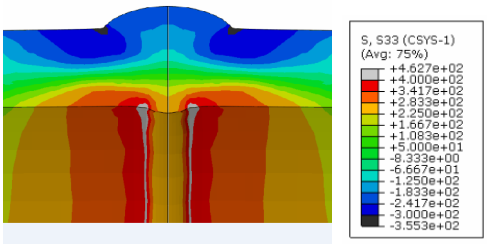

(b) Axial stress distribution in model b (temperature heat input)

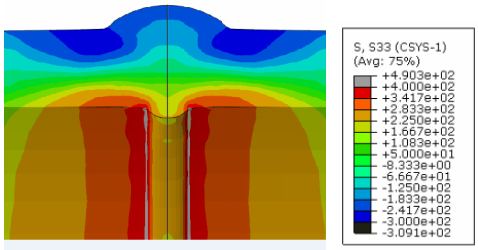

(c) Axial stress distribution in model b

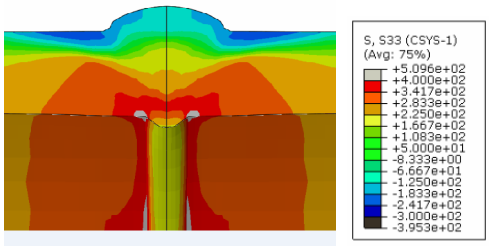

(d) Axial stress distribution in model c

Fig. 14. Axial residual stress distributions in models a, b and c at θ = 0°.

5. Analysis results

5.1 Thermal analysis results and verification

Temperature distribution induced by welding heat source is shown in Fig. 9. Note that all temperature contours are represented with axial symmetric part added for explanatory purposes. Gray region in the contour represents molten zone with temperature above 1454°C, which is the melting temperature of SUS347H. Fusion zones are compared in Fig. 10. Model a exhibits largest fusion zone and shows highest peak temperature among the models. Because of the axisymmetric feature of the model, heat conduction does not occur along circumferential direction. In addition, heating time for two-dimensional model is equal to the inverse of the welding speed, which is too small compared to those used in three-dimensional model, thus allowing limited time for heat conduction as well as heat convection, resulting in unrealistic, overestimated temperature

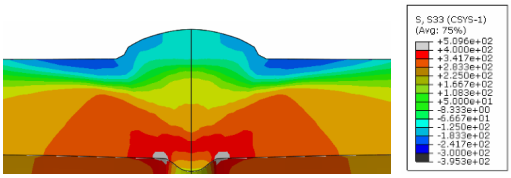

(a) Axial stress distribution in model c at θ = 0°

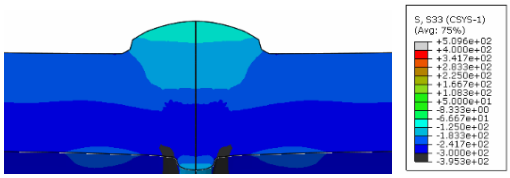

(b) Axial stress distribution in model c at θ = 90°

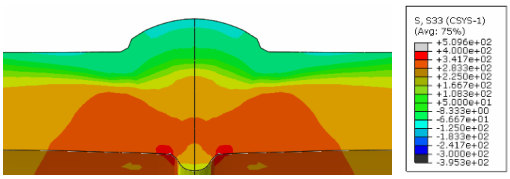

(c) Axial stress distribution in model c at θ = 180°

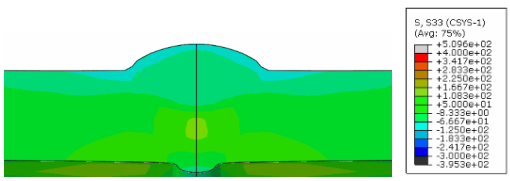

(d) Axial stress distribution in model c at θ = 270°

Fig. 15. Axial residual stress distributions in model c at θ = 0°, 90°, 180°, 270°.

field. Model c with temperature heat input shows lowest peak temperature because highest temperature is controlled to be the deposit temperature. Three-dimensional models show similar temperature distributions away from fusion zones.

Temperature history is measured at six different locations shown in Fig. 11. Bigger numbers represent measured locations and smaller numbers represent distances from second layer tip to the corresponding measured locations along axial direction. Location 4 was selected for comparison as it matches employed finite element models. Temperatures are measured and computed while weld torch moves along P1 shown in Fig. 3 and results are summarized in Fig. 12. Three-dimensional full model shows overall good agreement with measured data. Measured peak temperature is 691.3°C, while computed peak temperature using model c is 721.0°C. Two dimensional axisymmetric model has the lowest peak temperature of 628.9°C. Highest peak temperature was computed in three-dimensional half model with temperature heat input. Similar results can be found in the study by Vakili-Tahami et al. [4] in terms of peak temperatures and cooling rates.

5.2 Mechanical analysis results and verification

Equivalent stress distribution is shown in Fig. 13. Stress

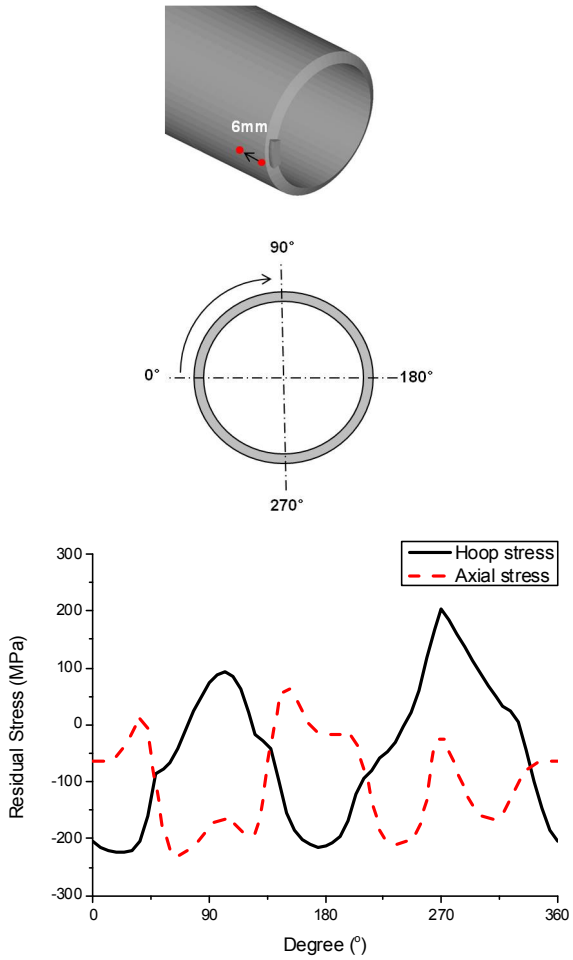

Fig. 16. Axial and hoop residual stress distributions in model c along circumferential path.

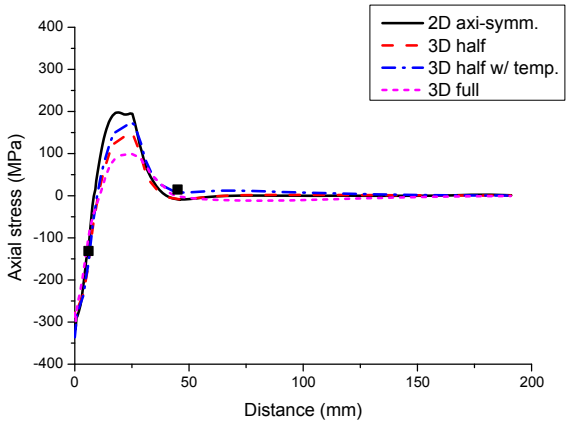

(a) Computed and measured axial residual stresses along axial path

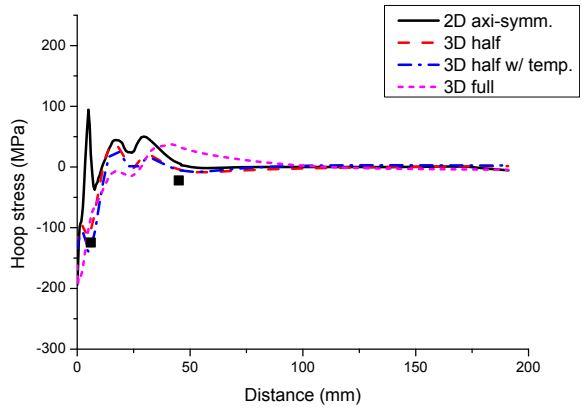

(b) Computed and measured hoop residual stresses along axial path

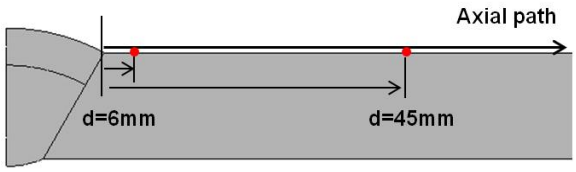

Fig. 17. Axial and hoop residual stress distributions in model c along axial path.

concentration is observed near the weld bead, and away from weld center plane, stress decreases to initial state. Axial stress distribution on 0°-180° surfaces is compared in Fig. 14. All four models show similar trend in the weld region, i.e., compressive stresses on the outer surface and tensile stress on the inner surface due to the weld sequence. Similar axial stress distributions are observed in three-dimensional half symmetry models, but the model with temperature heat input shows higher compressive and tensile stresses at the weld tips. Differences in models b and c are mainly due to the complicated weld pass configuration that model c has.

Axial residual stress distributions computed at four different sections ($\theta = 0°$, $\theta = 90°$, $\theta = 180°$, $\theta = 270°$) using the three dimensional full model are shown in Fig. 15. Each section shows different stress distribution. In case of section at $\theta = 90°$, compressive stress dominates the weld bead and its vicinity and no tensile stresses are found. In addition, stress distributions are compressive-compressive on respective inner, outer surface, which cannot be seen from weldments manufactured by simple, one-through pass welding. Weld start/stop effects are clearly shown in Fig. 16. Axial and hoop residual stresses are measured 6 mm from weld tip on outer surface along a complete circumferential path. Stress components were properly transformed to a cylindrical coordinate. Both axial and hoop stresses are fluctuating with large amplitudes from compressive to tensile distributions. Compared to the results by Dong et al. [8] and Barsoum et al. [5], in which the start/stop effect were relatively small, obtained results show large start/stop effects in that no stress plateau are found. Peak stresses in the plot seem to alternate at every 90° due to the start/stop position assumed in Fig. 3.

Axial and residual stresses obtained from employed finite element models are compared in Fig. 17. Measured stresses using XRD method are also shown in both plots. Measured locations are 6 mm and 45 mm from weld tip, respectively, as shown in Fig. 17. Stresses are obtained at $\theta = 47°$ section and along axial direction from weld tip on the outer surface to the

end of the tube. Both of the plots indicate that two-dimensional axisymmetric model overestimates stresses. Similar results are obtained by Duranton et al. [10] in which three-dimensional finite element model is employed to compute residual stresses in girth-welded SUS316L pipe. Computed and measured axial stresses are relatively in good agreement, including two-dimensional results. In contrast with axial stress, hoop stress computed using two-dimensional model showed large difference compared to those from other models. Peak hoop stress of two-dimensional model is computed to be 94.3 MPa at d = 5 mm, while model b has -113.74 MPa, model b with temperature heat input has -139.13 MPa and model c has -103.47 MPa.

6. Conclusions

In an attempt to develop a well defined numerical model that can take into consideration weld start/stop effects on welding residual stress distributions, a series of finite element analyses were carried out using three finite element models. Temperature histories and residual stresses were computed using each model and the results were compared and verified by measurements. The following conclusion can be drawn:

(1) For a three-dimensional full model, large fluctuation in stresses along circumferential direction was observed, indicating that the multiple weld start/stop process has significant effects on final weld residual stress distributions. The results suggest that three-dimensional models that can consider weld the star/stop effects have to be employed to obtain agreeable results.

(2) Two-dimensional axisymmetric model shows poor capabilities in predicting temperature histories and residual stresses in the presence of multiple weld start/stop. Residual stresses near the weld are overestimated compared to those by three-dimensional models. Moreover, a numerical model formulated under axisymmetric hypothesis cannot, by nature, capture the circumferential features of model behavior.

(3) Three-dimensional finite element model that has only axial symmetry in this work showed relatively acceptable performance in estimating temperature and residual stress distributions compared to other two- and three-dimensional models; therefore, this model can be employed for further analysis as numerical modeling of PWHT.

Acknowledgment

This work was financially supported by the Korea Institute of Energy Technology Evaluation and Planning (No. 2013101010170D), South Korea.

References

[1] J. Erneman, M. Schwind, P. Liu, J.-O. Nilsson, H.-O. Andren and J. Agren, Precipitation reactions caused by nitrogen uptake during service at high temperatures of a niobium stabilised austenitic stainless steel, *Acta Materialia*, 52 (2004) 4337-4350.

[2] D. Deng and D. Murakawa, Numerical simulation of temperature field and residual stress in multi-pass welds in stainless steel pipe and comparison with experimental measurements, *Computational Materials Science*, 37 (2006) 269-277.

[3] B. Brickstad and B. L. Josefson, A parametric study of residual stresses in multi-pass butt-welded stainless steel pipes, *Pressure Vessels and piping,* 75 (1998) 11-25.

[4] J. Xua, X. Jia, Y. Fan, A. Liu and C. Zhang, Residual stress analyses in a pipe welding simulation: 3D pipe versus axisymmetric models, *Procedia Materials Science,* 3 (2014) 511-516.

[5] Z. Barsoum and A. Lundback, Simplified FE welding simulation of fillet welds – 3D effects on the formation residual stresses, *Engineering Failure Analysis,* 16 (2009) 2281-2289.

[6] V.-T. Farid and Z.-A. Ali, Numerical and experimental investigation of T-shape fillet welding of AISI 304 stainless steel plates, *Materials and Design,* 47 (2013) 615-623.

[7] L. Tan, J. Zhang, D. Zhuang and C. Liu, Influences of lumped passes on welding residual stress of a thick-walled nuclear rotor steel pipe by multipass narrow gap welding, *Nuclear Engineering and Design,* 273 (2014) 47-57.

[8] D. Deng and S. Kiyoshima, FEM prediction of welding residual stresses in a SUS304 girth-welded pipe with emphasis on stress distribution near weld start/end location, *Computational Materials Science,* 50 (2010) 612-621.

[9] J. N. DuPont and A. R. Marder, Thermal efficiency of arc welding processes, *Welding Research Supplement* (1995) 406-416.

[10] P. Duranton, J. Devaux, V. Robin, P. Gilles and J. M. Bergheau, 3D modeling of multipass welding of a 316L stainless steel pipe, *Materials Processing Technology,* 153-154 (2004) 457-463.

Wanjae Kim is a senior research engineer in Korea Electric Power Corporation Research Institute, Daejeon, South Korea. His research interests include developing computational methods and numerical models for power generation systems integrity evaluation and monitoring.